Optically injected lasers: The transition from class B to class A lasers

B. Kelleher,[1,2] S. P. Hegarty,[2] and G. Huyet[1,2]

[1]*Centre for Advanced Photonics and Process Analysis, Cork Institute of Technology, Cork, Ireland*

[2]*Tyndall National Institute, University College Cork, Lee Maltings, Dyke Parade, Cork, Ireland*

We investigate changes in several features of the stability diagram of an optically injected single mode laser as the ratio of the photon lifetime to the carrier lifetime is progressively increased from very low values to very high values. In particular we consider the creation of a region of phase-locked bistability, changes in the nature of codimension-2 bifurcation points, and the presence or otherwise of chaos in the system. We show that many of the features associated with high values of the aforementioned ratio also emerge for very low pump currents regardless of the ratio of the lifetimes.

I. INTRODUCTION

For many laser applications where phase control over the light is desirable, optical injection is an important process. A useful figure in studies of optically injected lasers is the stability diagram where the behavior of the slave laser is mapped using the injection rate and the detuning frequency (the frequency of the master minus that of the slave) as control parameters. While this diagram can be extremely complicated and can contain a multitude of bifurcations (see [1] and references therein), there are two in particular that control the gross features of the system. One is a saddle-node (SN) bifurcation, and one is a Hopf bifurcation. In Ref. [2] a detailed experimental study of this mapping was undertaken, and these results were shown to agree extremely well with the predictions of a rate equation model.

In Ref. [3] the authors introduced a naming convention for lasers based on the ratios of the relaxation times of the polarization, electric field, and carrier density. A class C laser is one in which one needs equations for all three, a class B laser is one in which the polarization may be adiabatically eliminated, and a class A laser is one in which only the electric field needs to be considered. Conventional semiconductor lasers are class B lasers [3], meaning they can be described by a two-dimensional rate equation model for the intensity of the electric field and the carrier density. Class B semiconductor lasers have an intrinsic dynamic known as the relaxation oscillations (ROs) of the laser describing the damped oscillations arising after perturbations from equilibrium. Class A lasers [3], on the other hand, are one-dimensional, and perturbations decay exponentially. When a class B laser is subject to optical injection, an equation for the phase of the electric field is also needed, and the system becomes three-dimensional. Similarly, one needs to include the phase in the optically injected class A rate equation model, and this becomes two-dimensional.

The two main factors determining the RO characteristics are the ratio of the photon lifetime to the carrier lifetime and the pumping current. For typical values of the pumping current it is this lifetime ratio that determines the behavior, and in conventional semiconductor lasers, this ratio is very small. A consequence of this is that the ROs are weakly damped. Because of the prevalence of semiconductor lasers in modern technology, these devices (and, consequently, the

weakly damped system) have been the focus of most studies. Studies of intermediate damping levels do not seem to have been undertaken, and from a practical point of view it is easy to understand why: conventional semiconductor lasers do not have such damping values. This has changed, however, with the advent of quantum dash and dot lasers, providing a practical motivation for an investigation of intermediate damping levels. In Refs. [4,5] a four-dimensional rate equation model specific to quantum dot material was considered, taking into account the influence of the wetting layer and Pauli blocking. Microscopic models of quantum dot systems have also been investigated in Ref. [6] and under the influence of optical injection in Ref. [7]. The behavior of optically injected quantum dash lasers has been considered in Refs. [8,9]. In Ref. [8] the standard semiconductor laser rate equation model was used with the addition of an effective gain compression parameter to model the material dynamics.

Several unique features lead to the high damping in quantum dot devices, most significantly the occupation probability of the dots. For dots with an InAs active region the steady state occupation probability is close to 1, and this prevents prolonged relaxation oscillations via Pauli blocking, as shown in the rate equation modeling in Refs. [10,11]. Using parameters appropriate for InAs based quantum dot lasers, it was shown in Refs. [4,5] that the predictions of the model agreed well with experiment. Both yielded locking diagrams qualitatively very similar to that of a class A laser as considered in Ref. [12], with the performance of the optically injected quantum dot laser being significantly more stable than that of quantum well based devices but nonetheless displaying some regions of chaotic operation [5]. The presence of chaos means that the system is certainly not fully class A, where deterministic chaos cannot arise due to the low dimensionality. Thus it is of interest to consider the case where the standard rate equations are used but with the RO damping increased to consider when and how the class A features arise.

Theoretical and numerical investigations of the stability diagram typically amount to a bifurcation analysis of a rate equation model. The principal bifurcations in the stability diagram are Hopf and SN bifurcations. Together, these form the principal boundaries between phase-locked behavior and unlocked behavior. Of course, there are many other bifurcations that can be found in the system, and many of these have

been investigated in detail. These lead to many complicated dynamical features, such as excitability, multistability, and chaos. In this work we are concerned only with the main SN and Hopf bifurcations. We consider the transition from weakly damped to strongly damped class B behavior and finally to full class A behavior and describe the evolution of the gross features of the stability diagram. These features include the generation of a phase-locked bistability, the creation and annihilation of codimension-2 points in the system, and the presence of chaos. Finally, we show that for very low pump currents, the class A locking structure is generic. To begin with we compare a weakly damped class B laser with a class A laser.

II. COMPARISON OF CLASS A AND CLASS B STABILITY DIAGRAMS

The rate equation model for a class B semiconductor laser is

$$\dot{R} = NR + K\,\cos\phi, \tag{1}$$

$$\dot{\phi} = -\Delta + \alpha N - \frac{K}{R}\,\sin\phi, \tag{2}$$

$$\dot{N} = \gamma[P - N - (1 + 2N)R^2], \tag{3}$$

where R is the slave field amplitude, K is the injection rate, ϕ is the phase of the slave minus that of the master, Δ is the detuning (the frequency of the master minus that of the slave), α is the linewidth enhancement factor, N is the carrier density of the slave, γ is the ratio of the photon lifetime to the carrier lifetime, and P is the pumping current above threshold [13,14]. Time is expressed in units of the photon lifetime in these equations.

For quantum well and bulk lasers, the constant $\gamma \ll 1$. The class A limit is found by taking the opposite limit, namely, $\gamma \gg 1$. This allows an adiabatic elimination of the carrier equation, and the rate equations become

$$\dot{R} = N(R)R + K\,\cos\phi, \tag{4}$$

$$\dot{\phi} = -\Delta + \alpha N(R) - \frac{K}{R}\,\sin\phi, \tag{5}$$

where

$$N(R) = \frac{P - R^2}{1 + 2R^2}. \tag{6}$$

Typically, class A lasers such as gas lasers have low or even zero α. We retain the class A name but note that we will also consider nonzero α factors as in Ref. [7].

A typical stability diagram for a conventional class B semiconductor laser is shown in Fig. 1(a). Only the SN and Hopf bifurcations are shown (see [1] for further bifurcation details). A stability diagram for the class A system is shown in Fig. 1(b) (see [7] for further details). For the weakly damped system the Hopf bifurcation H prevents stable phase locking for a large portion of the area bounded by the SN bifurcation. The shaded (gray) area is that where the phase locking to the
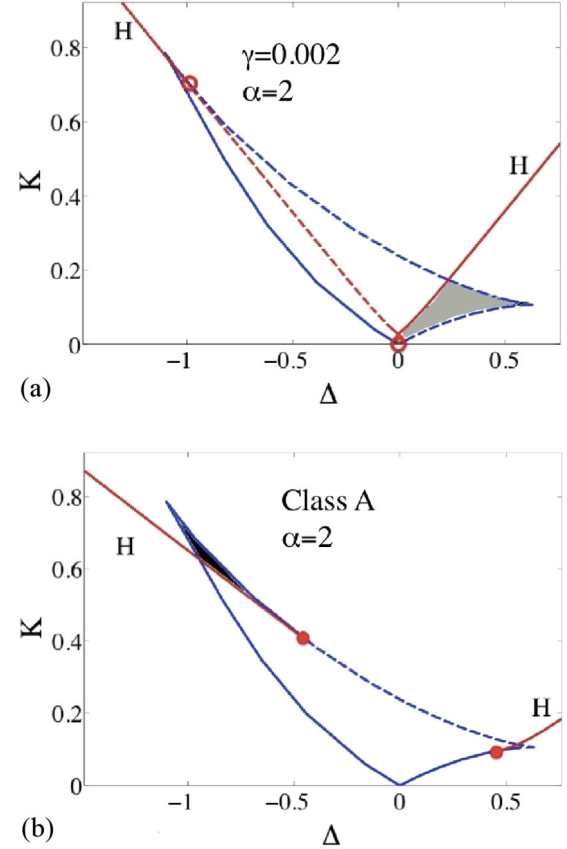

FIG. 1. (Color online) Two stability diagrams. H marks the Hopf bifurcation [red (light gray)] in each case, while the other curve is the SN bifurcation [blue (dark gray)]. (a) Weakly damped class B laser with $\gamma = 0.002$ and $\alpha = 2$. (b) Class A laser with $\alpha = 2$. In (a) the gray shaded region is that of unstable locking. In (b) the black shaded region is a region of bistability where two phase-locked solutions of different intensity coexist. Dashed lines represent unstable bifurcations. Solid lines represent stable bifurcations. The open red circles are codimension-2 FH points, and the solid red circles are codimension-2 BT points.

master is unstable. Stable phase locking at zero detuning is not even possible for some injection strengths. In contrast, this is always a stable detuning for class A lasers. The linewidth enhancement factor α also plays a large role in this instability [1]. In the class A diagram, the dark shaded area (black) is a region of phase-locked bistability. This region is one of the major differences between the systems, and we examine how it arises below. A second major difference between the systems is the nature of the codimension-2 intersections of the SN and Hopf bifurcations. In the weakly damped class B system these points are of fold-Hopf (FH) form, while in the class A system they are of Bogdanov-Takens (BT) form.

In this work we will consider only two values of α: $\alpha = 0$ and $\alpha = 2$. These are sufficient to display our essential points. While our main interest is in semiconductor laser systems, many of the results take especially simple forms in the $\alpha = 0$ case. This is also of interest for laser systems where low values of α are expected such as for gas lasers.
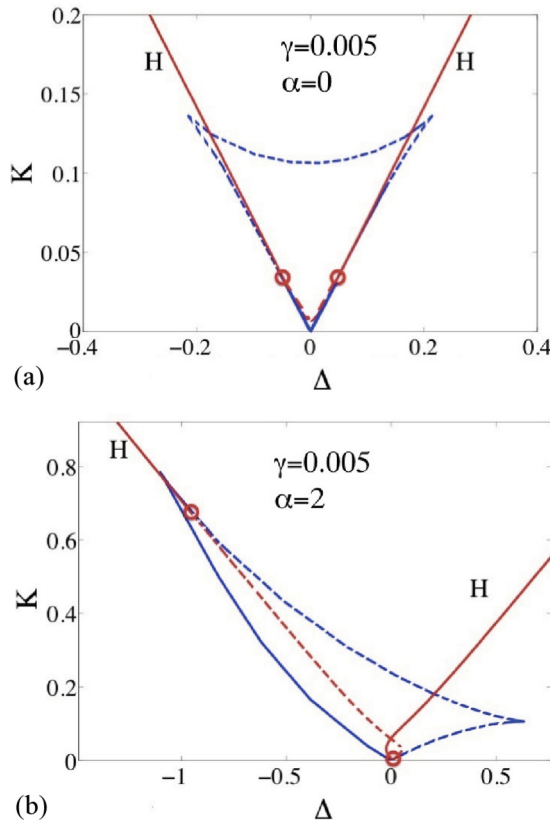
FIG. 2. (Color online) Two stability diagrams. H marks the Hopf bifurcation [red (light gray)] in each case, while the other curve is the SN bifurcation [blue (dark gray)]. In (a) $\alpha = 0$ and $\gamma = 0.005$. In (b) $\alpha = 2$ and $\gamma = 0.005$. The open red circles are codimension-2 FH points. Again, dashed lines are unstable bifurcations; solid lines are stable bifurcations.
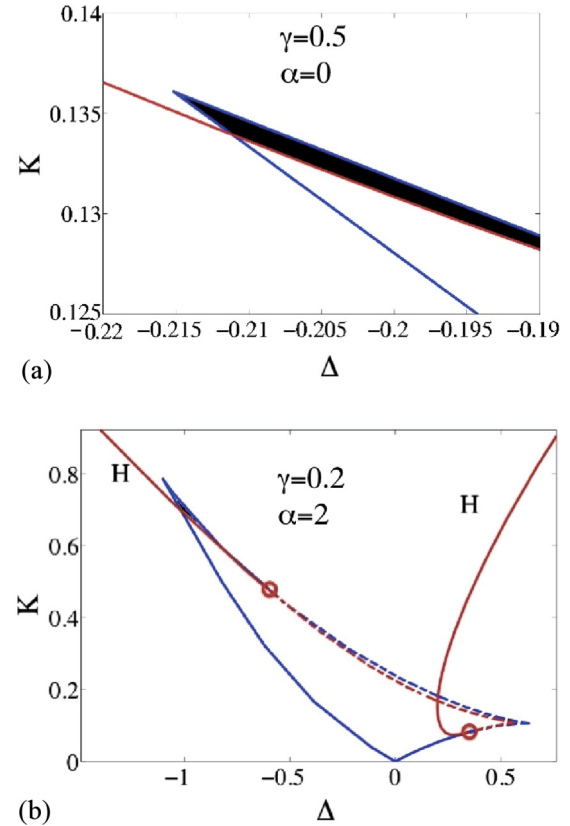

FIG. 3. (Color online) Two stability diagrams. In each H marks the Hopf bifurcation [red (light gray)], while the other curve is the SN bifurcation [blue (dark gray)]. (a) A portion of a stability diagram with a (shaded) region of bistability for $\alpha = 0$ and $\gamma = 0.5$. (b) The diagram for $\alpha = 2$ and $\gamma = 0.2$. The open red circles are codimension-2 FH points. Dashed lines represent unstable bifurcations. Solid lines represent stable bifurcations.

III. PHASE-LOCKED BISTABILITY

Bistability in general is a common feature in optically injected lasers. In some cases it results from an intrinsic property of the system, such as in semiconductor ring lasers, where there are two possible directions of propagation [15], vertical cavity surface emitting lasers, where there are two possible polarization states for the light [16–18], and two-mode lasers, where there are two possible emission wavelengths [19]. Despite the lack of such an intrinsic property to exploit, a phase-locked bistability in optically injected, single mode edge-emitting semiconductor lasers can also be obtained. Such a bistability has been observed for quantum dot lasers [4,5] at pumping currents well above threshold. It has also been studied for quantum well based lasers [20,21], but in these cases, observation of the bistability required a pump current only slightly above threshold. We return to such a limit later.

First, let us consider the simple $\alpha = 0$ case. Let us also fix $P = 0.5$. For low values of the damping there are two codimension-2 points, both of FH form, as shown in Fig. 2(a). One effect of increasing the value of α is that the diagram becomes asymmetric. Another is that the FH points migrate along the SN line and eventually pass the cusp, as shown in Fig. 2(b) (as also described in Ref. [1]). A result of this

migration is that another phase-locked solution can gain stability, thereby creating a region of phase-locked bistability between the SN line and the Hopf line. However, this region is either extremely small or vanishing for low values of γ.

Keeping $\alpha = 0$ but increasing γ instead, we find a similar migration of the FH point, again resulting in a bistable region. Such a region of bistability is shown in Fig. 3(a) for $\alpha = 0$ and $\gamma = 0.5$. Since this special case is symmetric, there are regions of bistability for both positive and negative detunings. As α is increased, the symmetry is eventually lost, but by continuity one must expect a positively detuned bistable region for some nonzero values of α. We do not pursue this topic further here as, experimentally, semiconductor lasers with such low values of α are not currently obtained, and we content ourselves with the prediction that one would expect two bistable regions for a sufficiently low α. As for the case of low damping this region is very small. Thus, while regions of bistability are possible for very low γ or very low α, they are extremely small. We now consider the effect of a moderate α and the effect of increasing γ.

As just described, the migration of the FH point resulting from an increase in γ can yield a region of phase-locked bistability, albeit initially an extremely small region. As γ is further increased, the FH point moves ever farther along

the SN curve, and the bistable region grows correspondingly. Figure 3(b) shows the stability diagram for $\alpha = 2$ and $\gamma = 0.2$, where a clear bistable region exists for negative detuning. (Figure 5 shows two further stability diagrams for yet higher values of γ with large bistable regions.) This does not continue indefinitely, however, and we see in the next section that, eventually, the bistable region will begin to contract in size as γ is increased. Nonetheless, it is quite striking that a general feature of the class A locking structure already exists even for relatively low values of γ.

Bistable behavior arising in this manner has been demonstrated for quantum dot lasers undergoing optical injection both experimentally and theoretically in Ref. [4], where the similarity to class A behavior was noted. We see now that this feature also arises from the conventional rate equations even for moderate damping values.

IV. CODIMENSION-2 POINTS: CREATION, COLLISION, AND ANNIHILATION

As already mentioned, for a weakly damped conventional class B semiconductor laser undergoing optical injection, the codimension-2 points formed by the intersection of the SN and Hopf bifurcations are of FH form. The existence of such points in the optically injected system was first identified in Ref. [22], and an analytic expression for the locations of the points was obtained. From the point of view of dynamics these points are extremely important organizing centers in the system and hence have been studied in great detail, with most studies focusing on the positively detuned point. In Ref. [23] the effect of the point on organizing the flows and dynamics in the system was studied in great detail. This point has also been the subject of several careful and detailed studies by Zimmermann and coworkers, such as in Ref. [24], where they examined the structure of resonance tongues near the FH point (for a fixed value of the relaxation times), and in Ref. [25], where homoclinic and heteroclinic bifurcations were investigated both numerically and theoretically. These studies provide many details regarding the deep bifurcation structure of the system near the FH point and of the orbits and flows in the phase space of the system. Our goal in this work is more modest: we aim to investigate only the gross codimension-2 structure and how the FH points disappear and the BT points appear as the ratio of the relaxation times is progressively increased.

That the codimension-2 points arising from the intersections of the SN and the Hopf bifurcations in the class A system cannot be of FH form but rather must be of BT form can be demonstrated using a simple counting argument. The characteristic equation is quadratic, and so there are only two eigenvalues per point. If one of these is zero, corresponding to the SN bifurcation, then there cannot simultaneously be a conventional Hopf bifurcation as there is only one other eigenvalue. Rather, the Hopf must meet the SN in a singularity with both eigenvalues equal to zero, that is, in a BT point. The question of how this transformation occurs is the basis of our next investigation. To investigate this we need to find the characteristic equation for the system by linearizing

Eqs. (1)–(3), yielding,

$$\lambda^3 + A_1\lambda^2 + A_2\lambda + A_3 = 0, \tag{7}$$

where the coefficients A_i are given by

$$A_1 = -2N + \gamma\left(\frac{1+2P}{1+2N}\right),$$

$$A_2 = -2N\gamma\left(\frac{1+2P}{1+2N}\right) + N^2 + 2\gamma(P-N) + (\Delta - \alpha N)^2,$$

$$A_3 = -2\gamma(P-N)[N - \alpha(\Delta - \alpha N)]$$
$$+ \gamma\left(\frac{1+2P}{1+2N}\right)[N^2 + (\Delta - \alpha N)^2], \tag{8}$$

as also shown in Ref. [13].

We first consider again the simplified $\alpha = 0$ system. The $\alpha = 0$ simplification allows us to find some simple analytic results and will aid understanding for the more general case. In Fig. 2(a) a stability diagram for $\alpha = 0$ and weak damping is shown. There are two FH points satisfying $A_1 = 0$, $A_3 = 0$ (corresponding to one zero eigenvalue). As γ is increased, the minimum of the Hopf bifurcation moves to ever higher injection strengths and eventually touches the SN bifurcation at a third codimension-2 point, as shown in Fig. 4(a). This third codimension-2 point is of BT form and by symmetry it must occur at $\Delta = 0$. We can find a simple expression for γ_{c1}, the critical value for this third codimension-2 point. The conditions for a BT point are $A_2 = 0$, $A_3 = 0$, and these yield

$$0 = 4N^2 + (3 - 2P)N - 2P, \tag{9}$$

$$\gamma_{c1} = \frac{N^2}{2}\left[N\left(\frac{1+2P}{1+2N}\right) - P + N\right]^{-1}. \tag{10}$$

Equation (9) defines the position of the SN line and is, of course, independent of γ. It allows us to find N for a given P. Equation (10) then allows us to find γ_{c1}. For $P = 0.5$ we find $\gamma_{c1} = 0.25$.

At this value of γ there are three codimension-2 points: two FH points and the newly created BT point, as shown in Fig. 4(a). By increasing the value of γ still further the BT point splits into two separate BT points, giving four codimension-2 points. Further increasing γ, the FH points migrate along the SN line towards the BT points and vice versa. The collisions of these different codimension-2 points take place in codimension-3 points, where $A_1 = 0$, $A_2 = 0$, and $A_3 = 0$. The values of γ for these points can be found from the coupled equations

$$\gamma_{c2} = \frac{4N^2 + 2N}{1 + 2P} \tag{11}$$

and

$$12N^3 + (12 - 4P)N^2 + (5 - 8P)N - 3P = 0, \tag{12}$$

and these are found at $\gamma_{c2} \approx 0.4108$ and at $\Delta \approx \pm 0.1545$. From this point on, the codimension-2 points associated with stable locking are of BT form. Continuing to increase γ, we find that the codimension-2 points continue to migrate. Eventually, the two FH points meet and mutually annihilate, after which there are only BT points. This annihilation occurs at $\gamma_{c3} = 0.5$ and $\Delta = 0$, as shown in Fig. 4(b), where only the

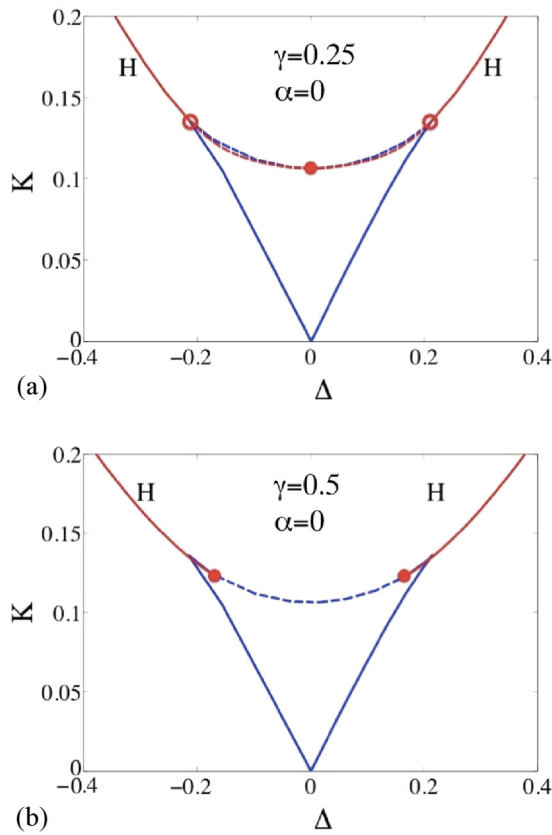FIG. 4. (Color online) Two stability diagrams for $\alpha = 0$. H marks the Hopf bifurcation [red (light gray)] in each case, while the other curve is the SN bifurcation [blue (dark gray)]. (a) shows the emergence of the (degenerate) BT point (solid red circle) coexisting with two FH points (open red circles) at $\gamma = 0.25$. (b) is for $\gamma = 0.5$, where the FH points have mutually annihilated and only BT points remain. Dashed lines are unstable, and solid lines are stable. The unstable part of the Hopf is not shown in (b) as it almost coincides with the SN line.
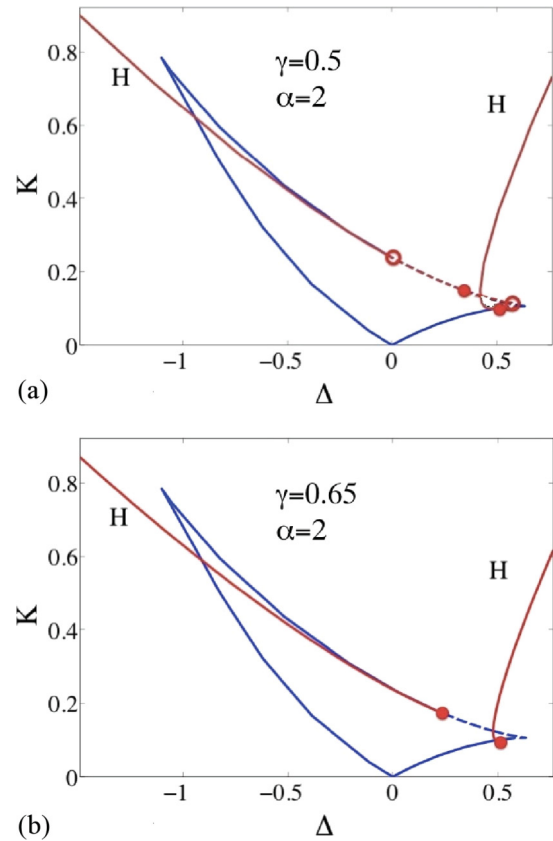

FIG. 5. (Color online) Two stability diagrams for $\alpha = 2$. H marks the Hopf bifurcation [red (light gray)] in each case, while the other curve is the SN bifurcation [blue (dark gray)]. In (a) four codimension-2 points coexist: two FH (open red circles) and two BT (solid red circles) at $\gamma = 0.5$. In (b) only the BT points for $\gamma = 0.65$ remain. The dashed (solid) lines are unstable (stable) bifurcations. The unstable part of the Hopf bifurcation is not shown in the second case. It is always close to the SN line.

stable part of the Hopf is shown. (Note that it is a coincidence that $\gamma_{c3} = P$ here; this is not true for other values of P.)

Of course, real semiconductor lasers have a nonzero α. While the details are different, we find that the qualitative picture developed above holds. Specifically, the diagram is, of course, asymmetric, but the creation of the BT points and the annihilation of the FH points still occur. For $\alpha = 2$ the first BT point is born at $\gamma \approx 0.2408$ and at $\Delta \approx 0.6311$. This first (degenerate) BT point splits into two separate BT points, which then migrate and collide with their respective FH points in codimension-3 bifurcations. For nonzero α these occur at different values of γ. At $\gamma \approx 0.3774$ we have the codimension-3 collision of the more positively detuned FH point at $\Delta \approx 0.5416$. At $\gamma \approx 0.5946$ and $\Delta \approx 0.2654$ we have the codimension-3 collision of the more negatively detuned FH point and a BT point. Up to this point the range of injection strengths over which the system has a phase-locked bistability grows with increasing γ. From this point, however, this region starts to shrink again since from here on this BT point moves to higher and higher injection strengths. The FH points are eventually mutually annihilated at $\gamma \approx 0.6409$ and $\Delta \approx 0.5097$.

Figure 5 shows two stability diagrams, one with four codimension-2 points and another where there are only BT points. Qualitatively, Fig. 5(b) is the same as the class A diagram shown in Fig. 1(b). Note that the size of the bistable region in this class B case is greater than that of the class A system.
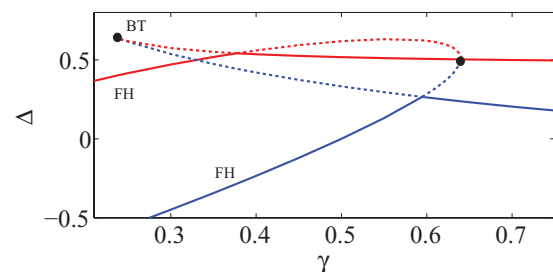

FIG. 6. (Color online) The evolution of the codimension-2 points with γ for $\alpha = 2$. The codimension-3 collisions of the BT and FH points are those points where solid lines become dashed and vice versa. The black dots mark the positions of the creation of the BT points (on the left) and the annihilation of the FH points (on the right).

Figure 6 shows the evolution of the FH and BT points as γ is increased. The creation of the BT points and the annihilation of the FH points are marked with black dots. The codimension-3 points where FH and BT points corresponding to the same steady states coincide are the points where solid lines become dashed and vice versa.

Even at the highest of these values of γ, the free-running laser is still an underdamped system. In fact, for $P = 0.5$ the system is underdamped for all $\gamma < 1$. For $\gamma > 1$ the system is overdamped, but even then it is far from the class A limit. Thus, another of the features typically associated with the class A system, the presence of BT points rather than FH points, is shown to arise at moderate damping levels in the class B system and, in particular, much earlier than the class A limit. Despite the similarities between even a moderately damped class B system and the class A system, some distinct differences remain. In particular, deterministic chaos cannot occur in the class A system as it is two-dimensional. However, it can and does arise in the class B system, even after the class A characteristic features have arisen, as we now show.

V. CHAOS

The focus of our analysis so far has been on the locking region and the determination of stable and unstable boundaries. We consider some of the unlocked behavior in this section. It is well known that chaos is encountered for weakly damped conventional semiconductor lasers undergoing injection [1,3]. (In fact, the generation of chaos was part of the motivation for introducing injection in Ref. [3].) As mentioned above, for the class A system deterministic chaos is impossible: there are only two dimensions. Nonetheless, even when many of the features of the class A diagram have been generated for the class B system, one may still encounter regions of chaotic behavior. We demonstrate this by explicitly simulating a chaotic time series for $\gamma = 0.38$. There is an appreciable region of bistability at this level, and BT points have already been generated. In fact, one of the codimension-3 collisions of an FH point and a BT point has already occurred, and so the more positively detuned codimension-2 point associated with stable locking is already of BT form. Despite this, chaotic regions can remain in the system. In Fig. 7 we show an intensity time series and a phase plot demonstrating chaotic behavior. Qualitatively, this is just like the case for optically injected quantum dot lasers where the Hopf and SN structure is reminiscent of class A lasers but chaotic regions are nonetheless observed [4,5]. As γ is further increased, the regions of chaos grow ever smaller.

VI. LOWER PUMP CURRENTS

A possible objection to the relevance of the analysis thus far is that the most interesting range of values for γ is $0.2 \lesssim \gamma \lesssim 0.6$. Although these are much less than the values needed to justify a full class A approximation, they are still significantly higher than the values obtained for conventional semiconductor lasers. A notable exception, of course, is the aforementioned quantum dot lasers.

An important point is that we have so far considered only one particular choice of the pump current, namely, $P = 0.5$. The RO properties of the system depend greatly
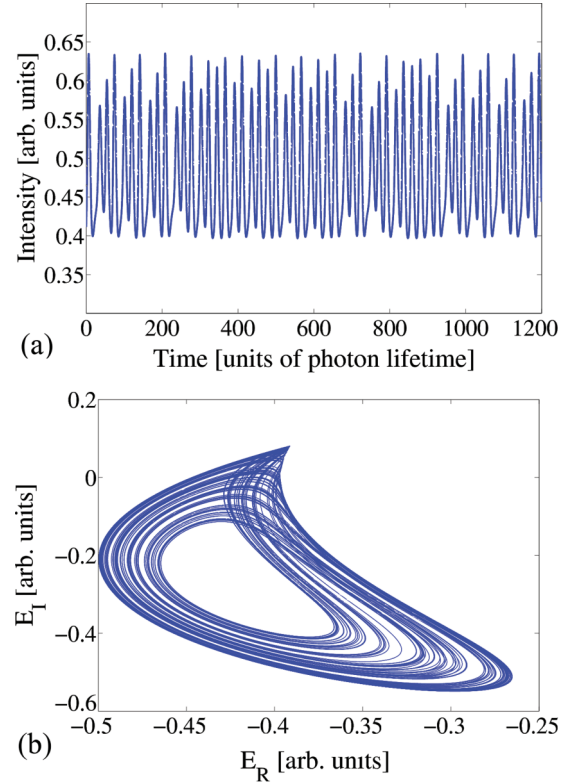

FIG. 7. (Color online) (a) Chaotic time series of the intensity and (b) the corresponding phase plot of the electric field. The parameters are $\Delta = 0.435$, $K = 0.099$, $\gamma = 0.38$, $P = 0.5$, and $\alpha = 2$.

on this particular parameter, and so one should consider more carefully how the system changes as it is varied. In Refs. [20] and [21] a low pump current was used to demonstrate a phase-locked bistability, and in Ref. [26] the existence of BT points at low pump currents was intimated. Let us look at this process a bit more closely. By examining the expressions for the RO parameters we can see why one might expect to find high damping phenomena at low current values. The RO frequency has the form $\Omega_{\mathrm{RO}} = \sqrt{2P\gamma - \gamma^2(\frac{1+2P}{2})^2}$, while the RO damping has the form $\Gamma_{\mathrm{RO}} = \gamma(\frac{1+2P}{2})$. Decreasing P towards $\gamma/8$, we have $\Omega_{\mathrm{RO}} \to 0$, while the damping
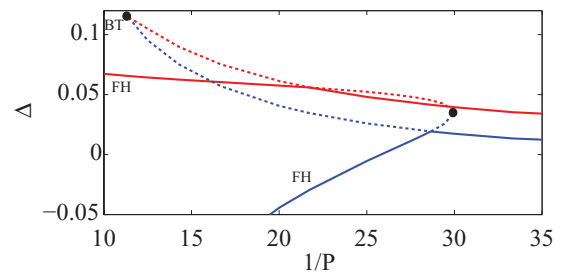

FIG. 8. (Color online) The evolution of the codimension-2 points with P for $\alpha = 2$. The codimension-3 collisions of the BT and FH points are those points where solid lines become dashed and vice versa. The black dots mark the positions of the creation of the BT points (on the left) and the annihilation of the FH points (on the right).
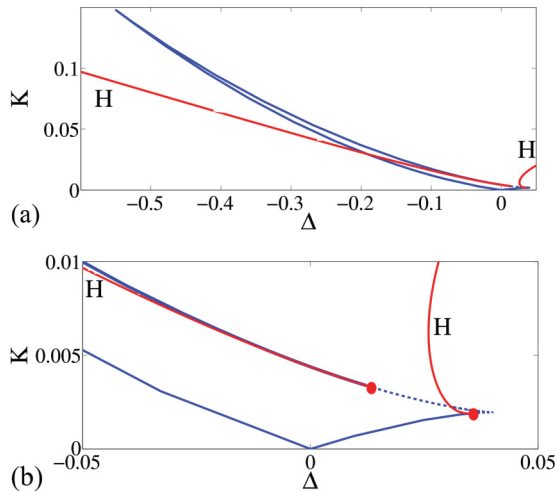
FIG. 9. (Color online) Stability diagram for the system with a low value of P. (a) shows the full extent of the SN bifurcation, while (b) shows a zoom of the low injection region. The similarity with the class A stability diagram is clear. The Hopf bifurcation curves [red (light gray)] are denoted with H, and the other curve is the SN bifurcation [blue (dark gray)]. Solid lines denote stable bifurcations, and dashed lines denote unstable bifurcations. Only the stable parts of the Hopf bifurcation are shown. The red dots show the positions of the codimension-2 BT points.

remains finite with $\Gamma_{RO} \rightarrow \gamma/2(1 + \gamma/4)$. This suggests that for $P \sim O(\gamma)$ even a conventional semiconductor laser may have some class A like characteristics. As P is decreased, the onset of BT points and bistability phenomena arise at correspondingly lower values of γ. For example, at $P = 0.1$ the BT points first arise at $\gamma = 0.0567$, while at $P = 0.05$ they arise at $\gamma = 0.0292$. By fixing γ and allowing P to decrease, one can mirror the sequence of behavior found when P was fixed and γ was increased. In Fig. 8 we fix $\gamma = 0.05$ and show the evolution of the codimension-2 points as P is decreased. The observed pattern is qualitatively the same as in Fig. 6. For high P values there are only FH points. At some critical P a pair of degenerate BT points is born. These points subsequently separate and migrate as P is decreased still further. As before, we have codimension-3 collisions of the BT and FH points, and eventually, the two FH points collide and are annihilated, after which there are only BT points.

We show a stability diagram with $\gamma = 0.05$ and $P = 0.03$ in Fig. 9. The codimension-2 points are of BT form, and there is a large region of bistability between two phase-locked states. The qualitative similarity to the conventional class A stability diagram is clear.

VII. CONCLUSIONS

In summary, we have considered the evolution of the stability diagram for optically injected semiconductor lasers as the RO damping is varied. Even for moderate values of γ the qualitative features of the class A locking diagram emerge. As the damping is increased we find the creation of codimension-2 BT points coexisting with codimension-2 FH points. As the damping is increased further, there are codimension-3 collisions of the FH and BT points and, eventually, the collision and mutual annihilation of the FH points, after which only the BT points remain. Large regions of phase-locked bistability also emerge. Nonetheless, we showed that even with the appearance of the general characteristics of the class A locking region, regions of chaotic behavior outside the locking region persist. These disappear in the class A limit. The presence of chaos outside a class A like locking region is qualitatively similar to experimental observations with optically injected quantum dot lasers. We also showed that for sufficiently low pump currents, a class A structure arises regardless of the value of γ. Of course, stochastic effects become very important for these low pump currents, and so an analysis of the effect of noise terms should be performed.

[1] S. Wieczorek, B. Krauskopf, T. B. Simpson, and D. Lenstra, Phys. Rep. **416**, 1 (2005).

[2] S. Wieczorek, T. B. Simpson, B. Krauskopf, and D. Lenstra, Phys. Rev. E **65**, 045207 (2002).

[3] J. R. Tredicce, F. T. Arecchi, G. L. Lippi, and G. P. Puccioni, J. Opt. Soc. Am. B **2**, 173 (1985).

[4] T. Erneux, E. A. Viktorov, B. Kelleher, D. Goulding, S. P. Hegarty, and G. Huyet, Opt. Lett. **35**, 937 (2010).

[5] B. Kelleher, D. Goulding, S. P. Hegarty, G. Huyet, E. A. Viktorov, and T. Erneux, in *Quantum Dot Devices*, Lecture Notes in Nanoscale Science and Technology, Vol. 13 (Springer, New York, 2012), pp. 1–22.

[6] K. Lüdge and E. Schöll, IEEE J. Quantum Electron. **45**, 1396 (2009); K. Lüdge, R. Aust, G. Fiol, M. Stubenrauch, D. Arsenijević, D. Bimberg, and E. Schöll, *ibid.* **46**, 1755 (2010).

[7] J. Pausch, C. Otto, E. Tylaite, N. Majer, E. Schöll, and K. Lüdge, New J. Phys. **14**, 053018 (2012).

[8] N. A. Naderi, M. Pochet, F. Grillot, N. B. Terry, V. Kovanis, and L. F. Lester, IEEE J. Sel. Top. Quantum Electron. **15**, 563 (2009).

[9] J. F. Hayau, O. Vaudel, P. Besnard, F. Lelarge, B. Rousseau, L. Le Gouezigou, F. Pommereau, F. Poingt, O. Le Gouezigou, A. Shen, G.-H. Duan, O. Dehaese, F. Grillot, R. Piron,

S. Loualiche, A. Martinez, K. Merghem, and A. Ramdane, *European Conference on Lasers and Electro-Optics 2009 and the European Quantum Electronics Conference. CLEO Europe - EQEC 2009* (IEEE, Piscataway, NJ, 2009), p. 1.

[10] D. O'Brien, S. P. Hegarty, G. Huyet, and A. V. Uskov, Opt. Lett. **29**, 1072 (2004).

[11] T. Erneux, E. A. Viktorov, and P. Mandel, Phys. Rev. A **76**, 023819 (2007).

[12] C. Mayol, R. Toral, C. R. Mirasso, and M. A. Natiello, Phys. Rev. A **66**, 013808 (2002).

[13] A. Gavrielides, V. Kovanis, and T. Erneux, Opt. Commun. **136**, 253 (1997).

[14] We note that in this formulation the α factor appears explicitly. The equations can also be formulated without an explicit appearance of α by including a detuning with the atomic frequency in a polarization equation and then adiabatically eliminating the polarization appropriately as in Ref. [22].

[15] W. Coomans, S. Beri, G. Van der Sande, L. Gelens, and J. Danckaert, Phys. Rev. A **81**, 033802 (2010).

[16] Z. George Pan, S. Jiang, M. Dagenais, R. A. Morgan, K. Kojima, M. T. Asom, R. E. Leibenguth, G. D. Guth, and M. W. Focht, Appl. Phys. Lett. **63**, 2999 (1993).

[17] I. Gatare, M. Sciamanna, M. Nizette, H. Thienpont, and K. Panajotov, Phys. Rev. E **80**, 026218 (2009).

[18] A. Hurtado, A. Quirce, A. Valle, L. Pesquera, and M. J. Adams, Opt. Express **18**, 9423 (2010).

[19] P. Heinricht, B. Wetzel, S. O'Brien, A. Amann, and S. Osborne, Appl. Phys. Lett. **99**, 011104 (2011).

[20] T. Erneux, A. Gavrielides, and V. Kovanis, Quantum Semiclassical Opt. **9**, 811 (1997).

[21] A. Hohl, H. J. C. van der Linden, R. Roy, G. Goldsztein, F. Broner, and S. H. Strogatz, Phys. Rev. Lett. **74**, 2220 (1995).

[22] G. L. Oppo, A. Politi, G. L. Lippi, and F. T. Arecchi, Phys. Rev. A **34**, 4000 (1986).

[23] H. Solari and G. L. Oppo, Opt. Commun. **111**, 173 (1994).

[24] C. Mayol, M. A. Natiello, and M. G. Zimmermann, Int. J. Bifurcation Chaos **11**, 2587 (2001).

[25] M. G. Zimmermann, M. A. Natiello, and H. G. Solari, Phys. D **109**, 293 (1997); Chaos **11**, 500 (2001).

[26] T. Erneux and P. Glorieux, *Laser Dynamics* (Cambridge University Press, Cambridge, 2010).